



Hydrothermal Synthesis and Characterization of LiMn_2O_4 as a Cathode Material for Rechargeable Lithium-Ion Batteries Applications

Noor M. Ali ^{1*}, Omar A. Al-Jubouri ¹, Muhammad H. Al-AL-TIMIMI ¹,

Huda T. Homad ¹ and Esmail Jalali Lavasani ²

¹Physics Department, College of Science, Diyala University

²University of Bucharest, Faculty of physics, 3nanosae

*nmask88@gmail.com

This article is open-access under the CC BY 4.0 license(<http://creativecommons.org/licenses/by/4.0>)

Received: 27 February 2024

Accepted: 19 May 2024

Published: 30 April 2025

DOI: <https://dx.doi.org/10.24237/ASJ.03.02.862D>

Abstract

This research involved the production of the spinel compound LiMn_2O_4 as the cathode active substance for Li-ion cells using the hydrothermal method. The field-emission scanning electron microscope (FESEM) was employed for an evaluative analysis of the external surface morphology of the synthesized material. The crystal structure of the spinel material was confirmed using X-ray diffractometry (XRD). The XRD pattern exhibited no signs of impurity peaks, confirming a singular crystal structure phase. As per the Scherrer equation, the crystal size was estimated at 12.65 nm. The energy-dispersive X-ray spectroscopy spectra for the equipped sample showed the existence of manganese and oxygen, and the concentrations were very close to the elemental composition used. Electrochemical attributes were investigated through galvanostatic charge–discharge cycling and cyclic voltammetry in a specific voltage range. The LiMn_2O_4 sample displayed a charge capacity of 111.6 mAhg^{-1} and a discharge capacity of 109.9 mAhg^{-1} . The Coulombic efficiency exhibited by this electrode was 98.4%.



After 100 cycles, the capacity retention was as high as 57.1%. The electrochemical impedance spectroscopy measurements of the LiMn_2O_4 electrode, including the electrolyte bulk resistance, charge transfer resistance, and Warburg Impedance, were 8.1 ohms, 127.5 ohms, and 0.86 ohms, respectively.

Keywords: Hydrothermal Method, CV, Warburg Impedance, The Coulombic efficiency.

Introduction

A lithium-ion battery is a type of rechargeable battery that relies on lithium ions as the primary component in its electrochemical process. Known for their high energy density and extended cycle life, these batteries are widely recognized as a leading energy storage solution for portable electronic apparatuses such as drones, cell telephones, Photography cameras, airPods, and laptops [1,2].

In the foreseeable future, there are numerous prospects for electric vehicles and hybrid electric vehicles outfitted with rechargeable batteries. The key requirements for rechargeable lithium-ion batteries include low cost, safety, high energy density, and environmental sustainability [3]. While (LiCoO_2) is commonly utilized as a cathode material due to its high energy density and cycling stability, it presents several drawbacks. These include its cost, toxicity, environmental concerns, thermal instability, limited cycle life, and lower specific capacity and operating voltage compared to some alternative cathode materials, all of which can constrain the energy density and performance of LiCoO_2 -based batteries [4,5]. Spinel lithium manganese oxide (LiMn_2O_4) emerges as a cost-effective and eco-friendly alternative cathode material capable of meeting field-use requirements and becoming a promising choice for commercial use, potentially replacing LiCoO_2 in high-power lithium-ion batteries [6-8]. However, cells utilizing spinel LiMn_2O_4 as a cathode substance are known to suffer from significant capacity loss during charge-discharge cycles or storage, particularly at great temperatures [9,10].

Utilizing spinel lithium manganese oxide in high-power systems like EVs and HEVs necessitates fast kinetic characteristics. Various Nano-structured substances with various



morphologies, like Nanorods, Spherical Nanoparticles, Nanosheets, and Nanowires, have been found operative in improving the kinetic characteristics of the spinel lithium manganese oxide (LiMn_2O_4) electrode [11, 12]. The creation manner significantly influences the chemical and physical features of nanostructured substances, with numerous synthesis routes developed for preparing LiMn_2O_4 nanomaterials, including sol-gel, Pechini, combustion, and hydrothermal techniques, etc. [13-15]. The cycling capability of LiMn_2O_4 is constrained by issues like Jahn-Teller distortion and manganese dissolution [16,17]. Consequently, numerous methods have been explored to boost the performance of spinel-type cathode materials through doping techniques. Various metal ions such as iron, zinc, cobalt, or nickel have been introduced to enhance electrical conductivity, stability, cycle longevity, and performance under harsh conditions, including elevated temperatures and high-current charging/discharging [18-21].

In this study, we conducted the synthesis and analysis of the structural and morphological characteristics of the active material utilized in cathodes for lithium-ion batteries, employing the hydrothermal method. Our primary objective is to elucidate the properties of the produced material and showcase its effectiveness in fabricating a cathode with unique electrochemical properties.

Experimental part

Synthesis of LiMn_2O_4 Nanoparticles

The approach was used to produce nanoparticles (LiMn_2O_4). The procedure unfolds as follows: We dissolve precise quantities of lithium chloride (LiCl), manganese chloride tetrahydrate ($\text{MnCl}_2 \cdot 4\text{H}_2\text{O}$), individually in deionized water within separate beakers. The mixture formed by the previous solutions was then transferred to a different heat-resistant container (such as a beaker), then continuously stirred using a magnetic stirrer until a homogeneous solution was achieved. In addition, Sodium hydroxide (NaOH) with a concentration of 1.25 moles per liter (125×10^{-2} M/L) is dissolved in (100 mL) of deionized water separately. It is then added dropwise to the metal salts solution at Twenty-seven degrees Celsius until the power of hydrogen reaches approximately (twelve and a half), ensuring the precipitation of every metal ion in the solution. After one hour of heating at a temperature of 90 degrees Celsius with continuous stirring, the heating is turned off, and the solution is allowed to cool to 27°C . The



second step of preparation method is going to treat by heat via hydrothermal method. The colloidal solution was moved to a (A volume of 250 milliliters) autoclave reactor lined with Teflon. Once tightly sealed, the autoclave is placed inside a furnace and heated to 200°C for a period of 10 hours. Subsequently, it is left to cool naturally to ambient temperature. The substance is subsequently washed repeatedly with deionized water using a multi-funnel setup to guarantee the elimination of salts and aid in drying at room temperature. The colloidal solution is subsequently subjected to multiple filtration cycles using de-ionized water until the pH reaches a neutral value of seven. The ultimate product is then placed within an oven at a heat of 70°C for duration of 4 hours. The final product placed to calcination in an air environment at 800°C for a total of 4 hours. The following chemical equations can elucidate the reaction that occurred.

Characterization

The supplier companies and models for XRD, FESEM, EDS, CV, EIS, and GCD respectively were: XRD 6000 from Shimadzu/Japan, Tescan Mira3, Tescan Mira3, model CT-3008, model WisEIS-8100 premium, and workstation CHI660E. The specifications of the autoclave reactor (Supplier: China) are as follows. The reactor shell is made of high-quality nonmagnetic stainless steel. The liner material is produced from PTFE (Poly Tetra Fluoroethylene), which is highly chemically resistant and resistant to acid, alkali, and various organic solvents. The parts of the reactor are the reactor body, reactor lid, bottom pad, top pad, liner, and liner lid. The maximum operating temperature, safe operating temperature, working pressure, and recommended heating and cooling rate are $\leq 250^{\circ}\text{C}$, 200°C , $\leq 3\text{MPa}$, and $\leq 5^{\circ}\text{C}/\text{min}$, respectively.

Results and Discussion

X-ray Diffraction Analysis

X-ray testing was performed on the samples prepared using the hydrothermal method. The XRD patterns presented in Figures (1) demonstrate the formation of a single-phase LiMn_2O_4 . The XRD data obtained from the samples closely matched those provided by the Joint Committee on Powder Diffraction Standards (JCPDS).



A detailed evaluation of all cell parameters had been undertaken for XRD analysis on the chemical LiMn_2O_4 . The sample reveal single-phase cubic spinel with the $Fd-3m$ space group and favorable orientations of eight characteristic peaks: (111), (311), (222), (400), (331), (511), (440), and (531). They are cataloged with JCPDs card no. 35-0782. This means the spinel LiMn_2O_4 has been prepared successfully using the hydrothermal technique in addition to no phase impurities were detected (absence of impurity phases). In the spinel LiMn_2O_4 structure, the tetrahedral positions (8a) are filled by lithium, the octahedral sites (16d) are occupied by manganese, and the (32e) sites host the oxygen ions, as documented in references [22, 23]. The sample were revealed by their strong and sharp reflections to be well crystallized. Depending on the X-ray diffraction results, these samples had been chosen in this study and calculate the lattice constant (a_{exp}), X-Ray density, Crystallite Size (D), in addition to Hopping length (\AA). The peak broadening validates the presence of nanosized particles. The experimental lattice parameter (a_{exp}) was determined by the following relation [24]:

$$a_{\text{exp}} = d\sqrt{h^2 + k^2 + l^2} \quad (1)$$

Where each plane's interplanar distance is represented by d , as well as (hkl) corresponds to Miller indices, D_{ave} computed the average crystallite size using the established Scherrer equation:

$$D_{\text{ave}} = \frac{K\lambda}{\beta \cos\theta} \quad (2)$$

D_{ave} represents the average size of crystallites, with K symbolizing the Scherrer constant ($K = 0.94$), where λ stands for the wavelength of the employed X-ray, β denotes the full width at half maximum, and θ represents the Bragg angle. The volume of the unit cell in its cubic structure is determined using equation (3), and equation (4) is utilized to calculate the X-ray density (ρ_x) based on XRD data.

$$V_c = a_{\text{exp}}^3 \quad (3)$$

$$\rho_x = \frac{ZM}{N_A V_c} \quad (4)$$

Z corresponds to the count of formula units within a unit cell (Z equal eight for the spinel system), where M signifies the molecular weight of the model, N_A stands for Avogadro's number, in addition to V_c denotes the cell's volume [24].



The distances for hopping, namely L_{A-A} , L_{B-B} , in addition L_{A-B} , between ions situated at the A-site and B-site, had evaluated using the expressions:

$$L_{A-A} = (a_{\text{exp}}\sqrt{3})/4 \quad (5)$$

$$L_{B-B} = (a_{\text{exp}}\sqrt{2})/4 \quad (6)$$

$$L_{A-B} = (a_{\text{exp}}\sqrt{11})/8 \quad (7)$$

L_{A-A} , L_{B-B} , plus L_{A-B} denote the distances corresponding to Tetra-tetra A-A, Octa-octa B-B, plus Tetra-octa A-B, respectively [25]. Table 1 presents the XRD calculations of the (111) phase for LiMn_2O_4 sample.

Table 1: XRD Calculation of LiMn_2O_4 Nanoparticles

Lattice constant		Molecular mass	X-ray density	crystallite size (D_{111})	Hopping length (\AA)		
a_{exp} (\AA)	V (\AA^3)	g.mol^{-1}	ρ_x (g/cm^3)	D_{ave} (nm)	L_{A-A}	L_{B-B}	L_{A-B}
8.2018	551.7312	180.814	4.353	12.65	3.5514	2.8997	3.4003

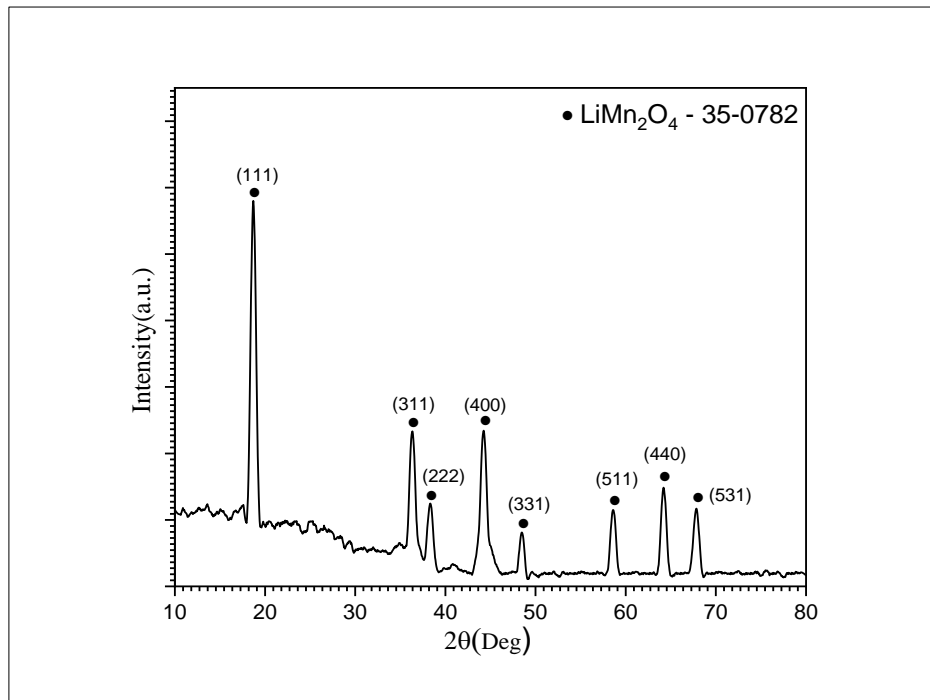


Figure 1: XRD results of the LiMn_2O_4 samples



FESEM image analysis of LiMn_2O_4

Figure 2 displays a Field Emission Scanning Electron Microscopy depiction of nanomaterial synthesized through the hydrothermal method, providing a densely concentrated view of the powdered sample and exhibiting fairly uniform grain dispersion (suitable particle size distribution). Furthermore, the particles produced exhibit a closely-packed as well harmonious arrangement. These images reveal approximately sphere-shaped particles characterized by sizes spread within several tens of nanometers. Consequently, the surface morphology and microstructure depicted in the images align well with the XRD data, illustrating the complementary nature of XRD and FESEM techniques in gaining a comprehensive understanding of the size and structure of materials.

The particles exhibit enhanced dispersion, and the bridging phenomenon is less pronounced. This elevated dispersion of particles facilitates their interaction with the electrolyte, consequently enhancing high-rate capability. All the samples can be described as comprising either small individual particles or larger aggregates of particles. Samples with smaller particle sizes offer the advantage of improved contact between the electrolyte-interface and electrode materials. This improved contact facilitates the intercalation in addition deintercalation of Li-ions during the procedure of charging and discharging [26, 27].

It's evident that the samples predominantly featured minimal pores among the particles. Additionally, cohesive forces including electrostatic, capillary, as well as Van der Waals forces led to interactions among the nanoparticles, ultimately resulting in their agglomeration. Histograms of particle size distributions were created using ImageJ software. The narrow distribution in particle size is depicted in Figure 2.

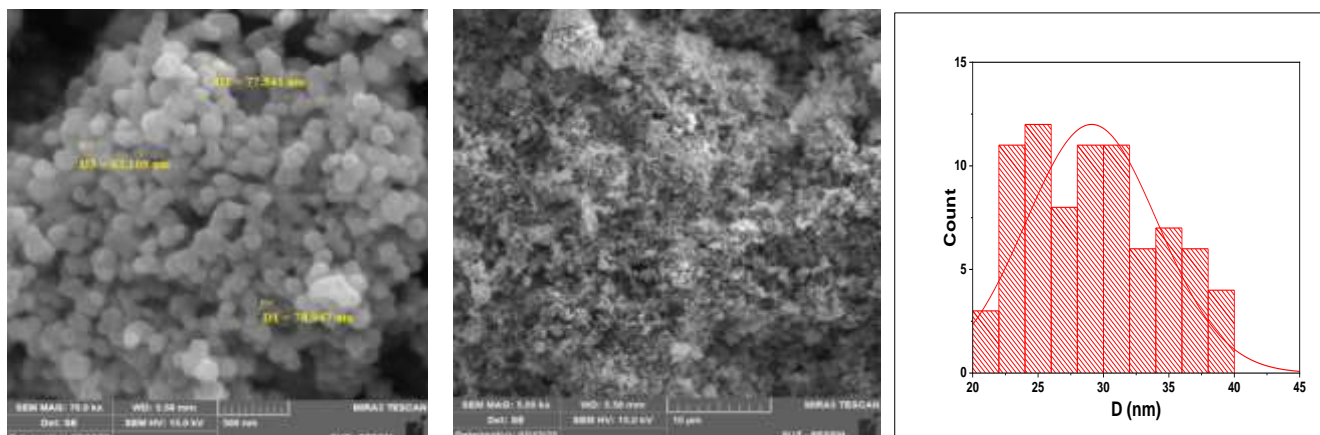


Figure 2: FESEM images and Histogram depicting particle size distributions of LiMn_2O_4 powder.

Energy Dispersive X-Ray Spectroscopy Investigation (EDS)

The composition of the prepared material was analyzed using the EDS technique across the zero to ten kilo-electron volt range. The EDS spectrum (Fig. 3) of the equipped model reveals the existence of Manganese and Oxygen, with concentrations closely matching the specified elemental composition. Additionally, no impurity peaks were observed in the EDS pattern. It's important to highlight that the detectors in the EDS device are calibrated to recognize radiations of specific energy; any energy below the calibrated value is undetectable by the detectors. Because Lithium-generated X-rays possess minimal energy, they cannot be detected using the radiation detector [28].

Several factors contribute to the difficulties in detecting lithium with EDS include lithium has a low atomic number ($Z=3$). Elements with low atomic numbers generally produce weak X-ray signals. The intensity of characteristic X-rays emitted during the interaction of the incident X-ray beam with lithium atoms is inherently low, making it difficult to distinguish the signal from the background noise. Moreover, the X-ray emission efficiency of lithium is relatively low compared to heavier elements. This means that the emitted X-rays from lithium are weak, further complicating their detection. Additionally, lithium X-rays are susceptible to absorption and scattering effects within the sample matrix. These phenomena lead to a reduction in the intensity of the emitted X-rays, affecting the signal-to-noise ratio and making it challenging to

accurately identify and quantify lithium. Besides, the sensitivity of EDS is influenced by the instrument's design and specifications. Many EDS systems are optimized for detecting mid to high atomic number elements, and their performance may be limited for light elements like lithium, especially when present in trace amounts. The X-ray peaks from lithium may overlap with other nearby peaks in the spectrum, particularly in complex samples. This overlap complicates the deconvolution of signals and introduces challenges in the accurate identification of lithium. Also, the form in which lithium is present in the sample can impact its detectability. If lithium is unevenly distributed or present in very small amounts, it may not produce a discernible signal. Additionally, certain sample preparation techniques may influence the visibility of light elements in EDS analysis [29,30].

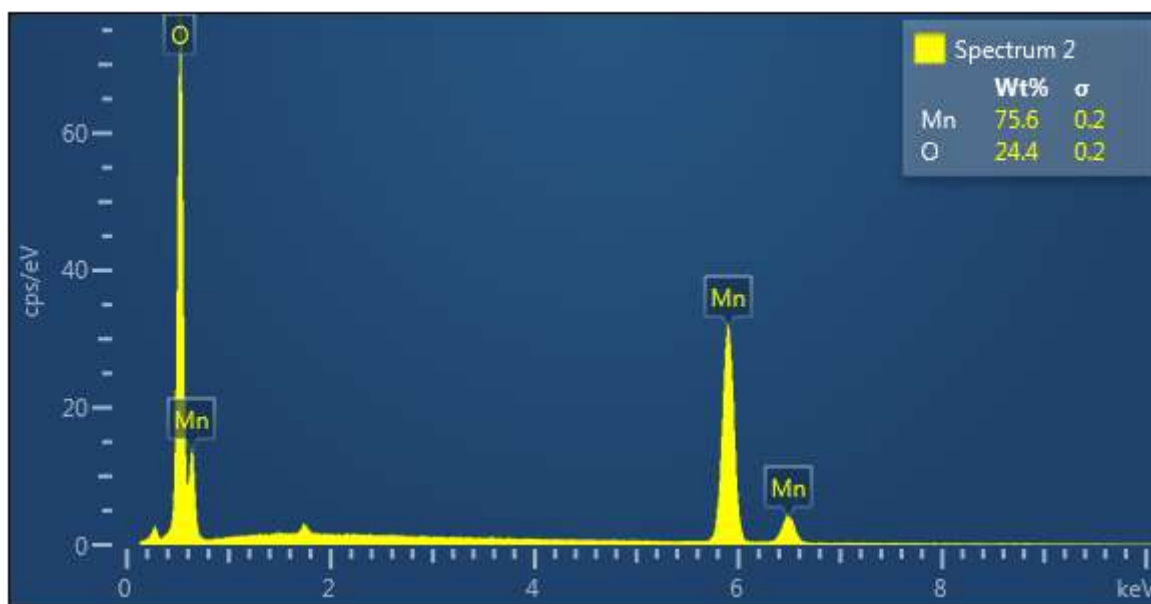


Figure 3: EDS analysis of LiMn_2O_4

Electrochemical properties of LiMn_2O_4

Figure 4 illustrates the cyclic voltammetry (CV) plots of the LiMn_2O_4 cathode synthesized via the hydrothermal method. The CV measurement was carried out in the potential range of 2.5 to 4.8 V. Cyclic voltammetry is a powerful and broad appealing electrochemical means typically adopted to meticulously study the reduction and oxidation processes of molecular species in



lithium-ion batteries. CV is also a beneficial technique to investigate the electron transfer-initiated chemical reactions in these energy storage devices [31].

According to (Figure 4), two distinct and well-defined pairs of the redox peaks are detected for the cathode fabricated via the hydrothermal technique. Both peaks are attributed to the intercalation/de-intercalation of the Li ions to or from the cathode material, a cathodic peak of 4.081/4.228 V and anodic peaks of 4.1246/4.279 V can be observed for this sample. The change in the intensity of the redox peaks and also their location with scan rate can be a good parameter to study the kinetics of lithium ion battery intercalation and de-intercalation process.

Several important factors that influenced the electrochemical performance, both positively and negatively, must be mentioned. The cyclic voltammetry exhibited two sets of distinct reversible redox peaks, characteristic of a stoichiometric spinel phase. These dual-stage procedures are associated with the arrangement of Li ions on half of the tetrahedral 8a sites, as outlined in existing literature, resulting in $\text{Mn}^{3+}/\text{Mn}^{4+}$ redox reactions [32]. Further indication of slight Mn dissolution is evident in the fact that the reduction current peaks nearly match the values of the oxidation current peaks. Samples displaying the greatest peak current and peak area demonstrate a discharge capacity superior to that of the other samples. Additionally, models with an anodic peak shift toward lower voltage and a cathodic peak shift toward higher voltage exhibit higher kinetics of lithium-ion diffusion [33]. The good structural arrangement, confirmed by the FESEM study and the higher surface area and shorter particle size, leads to an increase in electrochemical activity. However, the formation of a secondary phase at specific doping concentrations weakens the bonds in materials prepared in octahedrons, leading to a decrease in electrochemical activity. Samples with sharper and more symmetrical redox peaks demonstrate a higher rate of lithium-ion intercalation and deintercalation. Also, their smaller difference between redox potential and minimal electrode polarization during the charging/discharging process contributes to good cyclic performance [34-36].

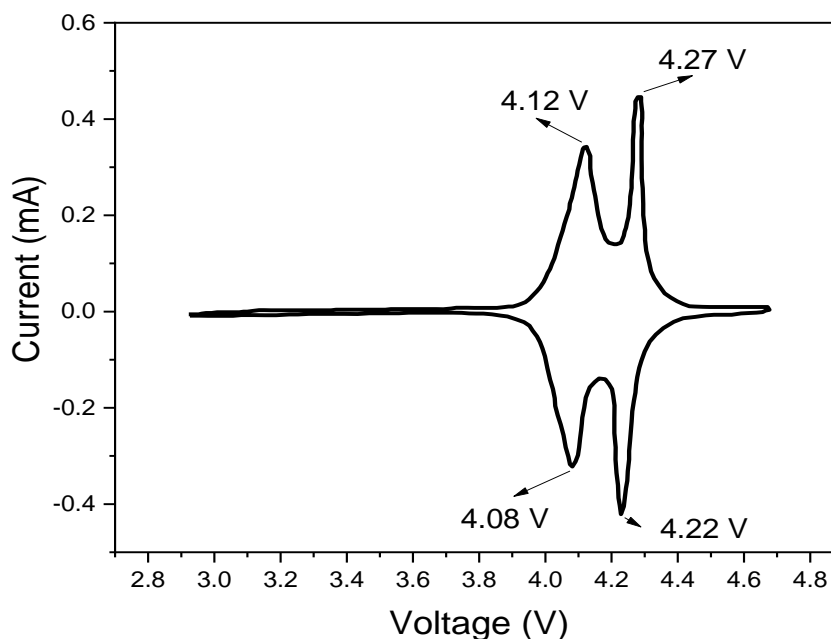


Figure 4: The CV for LiMn_2O_4 was obtained at a scanning rate of 1 mV/s within the specific voltage range.

Referring to the EIS test is essential, as it holds great importance and provides a comprehensive understanding of electrochemical properties. The principle of the EIS is application of a perturbation to an electro-chemical system in equilibrium or in steady state by using a sinusoidal signal (AC current or AC voltage) within a broad range of frequencies and recording the sinusoidal responses of the system toward the applied perturbation. It should be considered that the system under study is a linear time-invariant electrochemical system where the output signal has a linear relationship with the input signal as well as no change in the system's behavior is observed over time. EIS is a transfer function method modeling the output signal (AC voltage or AC current) to the input signal (AC current or AC voltage) within a broad range of frequencies [37].

The Nyquist plots of the cathodes in LIBs are commonly made up of a semicircle at medium-to-low frequency accompanied by a straight slope line located at low frequency. The intersection point of the curves and the Z_{re} axis at high frequency is imputed to the electrolyte's ionic conductivity (electrolyte bulk resistance or R_s). The semicircular varying from the medium to low frequency is ascribed to the charge transfer resistance between the



electrode/electrolyte and also the kinetic of the electrochemical reactions occurred in electrode (R_{ct}). The straight slope line known as the Warburg impedance (W_o) is relevant to the diffusion of lithium ions within the bulk of the host compound [38]. To elaborate further, a straight line in the plot indicates the diffusion or intercalation/de-intercalation manner of Li ions. The existence of a straight line suggests that Li ions can transfer simply from the cathode through the electrolyte and couple with electrons on the anode. A more steeply inclined straight line indicates a quicker diffusion pathway [39].

The EIS measurements of the LiMn_2O_4 electrode include the electrolyte bulk resistance or R_s , charge transfer resistance (R_{ct}), and Warburg Impedance (W_o). The values for R_s , R_{ct} , and W_o are 8.1 ohms, 127.5 ohms, and 0.86 ohms, respectively. The previous EIS parameters for the LiMn_2O_4 electrode indicate good diffusion of lithium ions within the electrode structure. These results align with the cyclic voltammetry (CV) data, where the LiMn_2O_4 electrode exhibited redox peaks. Furthermore, the distance between the pair of redox peaks was lower for this electrode, attributed to reduced polarization in the LiMn_2O_4 electrode [39].

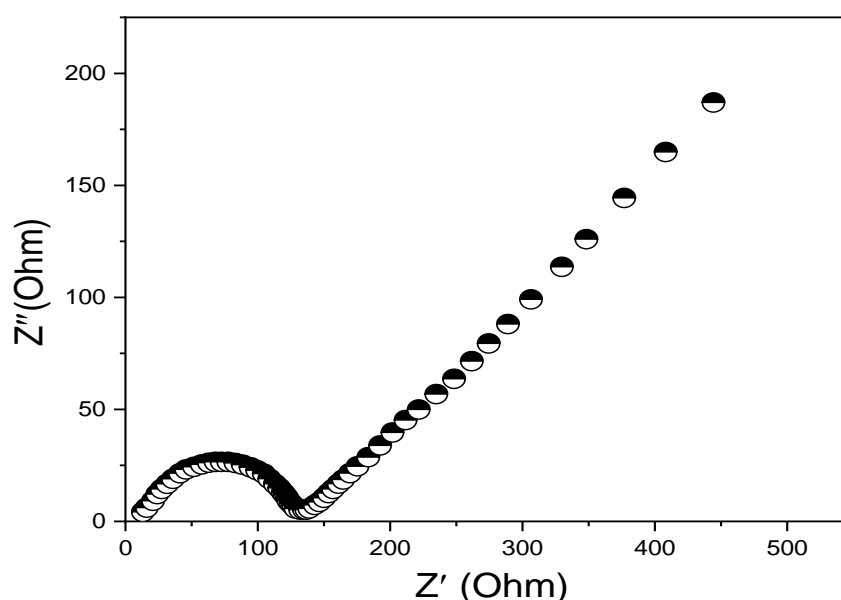


Figure 5: The Nyquist plot of the LiMn_2O_4 cathodes

Due to its significance in assessing battery performance, reference was also made to the charging and discharging processes. The LiMn_2O_4 cathode (in Figure 6), fabricated through the



hydrothermal process, displayed a charge capacity of 1116×10^{-1} mAh/g in addition to a discharge capacity of 1099×10^{-1} mAh/g. Additionally, the Coulombic-efficiency exhibited by this electrode was 98.4%. The Coulombic efficiency of a battery is a crucial metric in evaluating its performance over charge and discharge cycles. Coulombic efficiency is typically expressed as a percentage and is calculated by comparing the amount of charge delivered during discharge to the amount of charge supplied during charging. It is important to note that achieving a high Coulombic efficiency indicates minimal capacity fade between discharge and charge cycles. The superior electrochemical performance of the hydrothermal-based LiMn_2O_4 cathode can be attributed to the adoption of this method, which resulted in a cathode material with a structure that facilitates the transportation of lithium ions and enhances the movement of charges within the electrode. This improvement in Li ion diffusion is supported via EIS and CV measurements [32,40].

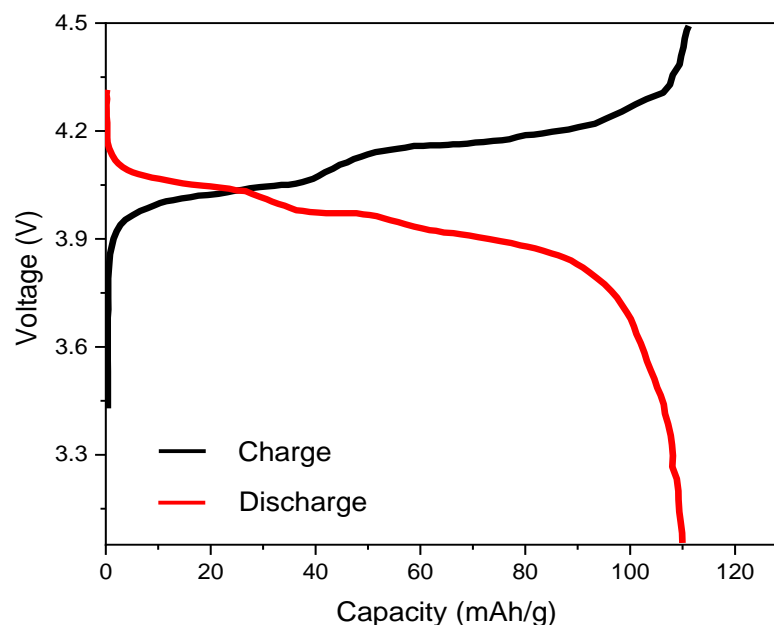


Figure 6: The initial charge/discharge cycle of the half cells composed of lithium counter electrode and LiMn_2O_4 as the working electrode recorded in the voltage of 2.0 to 4.8 V and the C-rate of 0.1.



Finally, the measurements were carried out using half-cells consisting of the lithium as the counter electrode and LiMn_2O_4 cathode material as the working electrode. The cycling performance of the electrodes was evaluated using a Neware multi-channel battery tester. The cycle life of a battery can be defined as the number of charging and discharging cycles that a battery can achieve before its capacity is completely depleted. A Li-ion battery with high performance should be able to keep its capacity constant even after several charging and discharging cycles. The cycle life of Li ion cells (batteries) immensely relies on the structural stability of the active materials of the electrode during the charge and discharging process.

The one produced by the hydrothermal technique delivered higher capacity retention after 100 cycles. Accordingly, the LiMn_2O_4 electrode showed capacity retention of 57.1% (Figure 7). As evidenced by these analyses, the LiMn_2O_4 electrode showed low in polarization and charge transfer resistance, which can be attributed to its good structure to easily transport the lithium ions within the electrode. The rapid movement of lithium ions within the fabricated electrode resulted in decreased polarization and improved conductivity [3, 41].

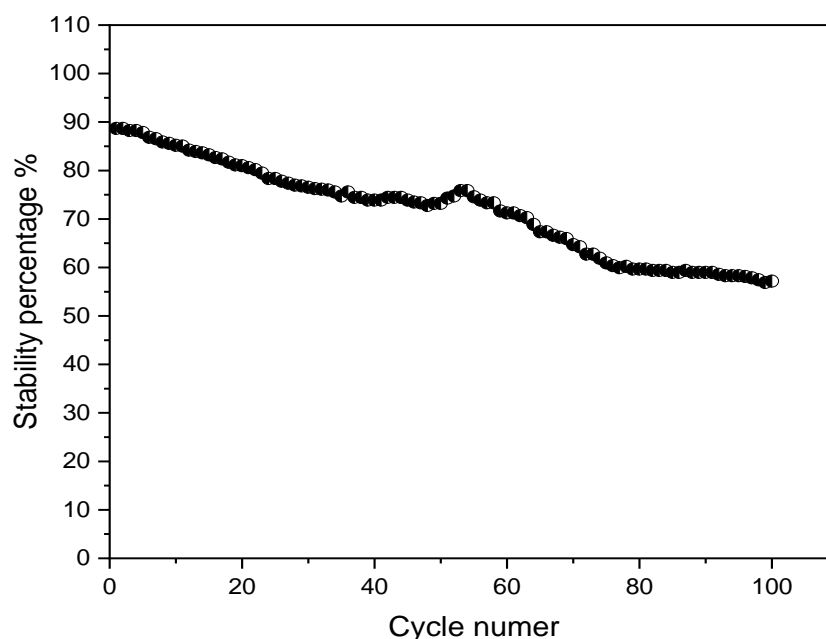


Figure 7: The stability percentage versus the cycle number of the LiMn_2O_4 cathode materials after 100 cycles in the voltage varying from 2.0 to 4.8 V and the C-rate of 0.1



At the end of the project, it is necessary to provide actionable suggestions regarding the significant influences on the prepared cathode material. Various factors affect battery electrochemical performance, including nanoparticle size and shape, as well as cathode material preparation temperature. Optimizing the preparation temperature is vital for tailoring cathode material properties to specific battery applications while maintaining stability and integrity. Nanoparticles, often possessing larger surface areas compared to larger particles of the same material, enhance battery performance by facilitating more active sites for electrochemical reactions. The shape of nanoparticles influences ion diffusion within the cathode material, with rod-shaped nanoparticles improving ion diffusion paths. Additionally, nanoparticle shape affects the structural stability of the cathode material, thereby impacting cycle stability and battery life. Smaller nanoparticles in battery cathodes increase surface area and enable faster ion diffusion, thereby enhancing charge and discharge rates. Controlling nanoparticle size is crucial for improving battery electrochemical performance [42, 43].

Conclusions

The hydrothermal method was employed to effectively manufacture LiMn_2O_4 for application as an electrode in Li-ion batteries. Structural as well as morphological tests have shown that it is possible to produce these materials with spinel structures characterized by high crystallinity and well-defined compositions. The electrochemical performance of these materials was examined through various analyses, including cyclic voltammetry, electrochemical impedance spectroscopy, initial charge/discharge cycles, and capacity retention measurements. The method used to prepare electrode materials significantly influences the structure, morphology, and surface characteristics of the particles. Consequently, these factors can lead to materials with improved conductivity, enhanced structural stability, and a favorable electrode-electrolyte interface. This, in turn, contributes to better charge retention over the battery's lifetime.

Source of funding: This study did not get any special funding.

Conflicts of Interest: The authors declare there are no conflicts of interest.

Acknowledgments

The authors express their gratitude to the University of Diyala, College of Science, Department of Physics, for furnishing the necessary tools, materials, and support for this paper.



References

- [1] K. Kang, Y. S. Meng, J. Breger, C. P. Grey, G. Ceder, Electrodes with high power and high capacity for rechargeable lithium batteries, *Science*, 311(5763), 977-980(2006), DOI(<https://doi.org/10.1126/science.1122152>)
- [2] F. Wu, J. Maier, Y. and Yu, Guidelines and trends for next-generation rechargeable lithium and lithium-ion batteries, *Chemical Society Reviews*, 49(5), 1569-1614(2020), DOI(<https://doi.org/10.1039/C7CS00863E>)
- [3] H. Du, Y. Wang, Y. Kang, Y. Zhao, Y. Tian, X. Wang, B. Li, Side Reactions/Changes in Lithium-Ion Batteries: Mechanisms and Strategies for Creating Safer and Better Batteries, *Advanced Materials*, 2401482(2024), DOI(<https://doi.org/10.1002/adma.202401482>)
- [4] B. Xu, D. Qian, Z. Wang, Y. S. Meng, Recent progress in cathode materials research for advanced lithium ion batteries, *Materials Science and Engineering: R: Reports*, 73(5-6), 51-65(2012), DOI(<https://doi.org/10.1016/j.mser.2012.05.003>)
- [5] J. B. Goodenough, K. S. Park, The Li-ion rechargeable battery: a perspective, *Journal of the American Chemical Society*, 135(4), 1167-1176(2013), DOI(<https://doi.org/10.1021/ja3091438>)
- [6] C. Wan, M. Wu, D. Wu, Synthesis of spherical LiMn_2O_4 cathode material by dynamic sintering of spray-dried precursors, *Powder technology*, 199(2), 154-158(2010), DOI(<https://doi.org/10.1016/j.powtec.2009.12.017>)
- [7] I. Taniguchi, N. Fukuda, M. Konarova, Synthesis of spherical LiMn_2O_4 microparticles by a combination of spray pyrolysis and drying method., *Powder Technology*, 181(3), 228-236(2008), DOI(<https://doi.org/10.1016/j.powtec.2007.05.011>)
- [8] H.W. Chan, J.G. Duh, S.R. Sheen, LiMn_2O_4 cathode doped with excess lithium and synthesized by co-precipitation for Li-ion batteries, *Journal of Power Sources*, 115, 110-118(2003), DOI([https://doi.org/10.1016/S0378-7753\(02\)00616-X](https://doi.org/10.1016/S0378-7753(02)00616-X))
- [9] Y. Xia, T. Sakai, T. Fujieda, X. Q. Yang, X. Sun, Z. F. Ma, M. Yoshio, Correlating Capacity Fading and Structural Changes in $\text{Li}_{1+y}\text{Mn}_{2-y}\text{O}_{4-\delta}$ Spinel Cathode Materials:



- A Systematic Study on the Effects of Li/Mn Ratio and Oxygen Deficiency, Journal of The Electrochemical Society, 148(7), A723(2001), DOI([10.1149/1.1376117](https://doi.org/10.1149/1.1376117))
- [10] G. Zhang, X. Wei, S. Chen, G. Han, J. Zhu, H. Dai, Investigation the degradation mechanisms of lithium-ion batteries under low-temperature high-rate cycling, ACS Applied Energy Materials, 5(5), 6462-6471(2022), DOI(<https://doi.org/10.1021/acsaem.2c00957>)
- [11] D. K. Kim, P. Muralidharan, H. W. Lee, R. Ruffo, Y. Yang, C. K. Chan, Y. Cui, Spinel LiMn_2O_4 nanorods as lithium ion battery cathodes, Nano letters, 8(11), 3948-3952(2008), DOI(<https://doi.org/10.1021/nl8024328>)
- [12] J. He, S. Zhuang, Z. Wang, G. Sun, X. Pan, Y. Sun, F. Tu, Facile preparation of regular truncated octahedral LiMn_2O_4 cathode with high rate cyclability and stability for Li-ion batteries, Journal of Alloys and Compounds, 943, 169162(2023), DOI(<https://doi.org/10.1016/j.jallcom.2023.169162>)
- [13] C. J. Curtis, J. Wang, D. L. Schulz, Preparation and Characterization of LiMn_2O_4 Spinel Nanoparticles as Cathode Materials in Secondary Li Batteries, Journal of the Electrochemical Society, 151(4), A590(2004), DOI([10.1149/1.1648021](https://doi.org/10.1149/1.1648021))
- [14] K. Du, H. Zhang, Preparation and performance of spinel LiMn_2O_4 by a citrate route with combustion, Journal of alloys and compounds, 352(1-2), 250-254(2003), DOI([https://doi.org/10.1016/S0925-8388\(02\)01165-9](https://doi.org/10.1016/S0925-8388(02)01165-9))
- [15] S. Nieto, S. B. Majumder, R. S. Katiyar, Improvement of the cycleability of nanocrystalline lithium manganate cathodes by cation co-doping, Journal of power sources, 136 (1), 88-98(2004), DOI(<https://doi.org/10.1016/j.jpowsour.2004.05.020>)
- [16] X. Li, Y. Xu, C. Wang, Suppression of Jahn–Teller distortion of spinel LiMn_2O_4 cathode, Journal of Alloys and Compounds, 479(1-2), 310-313(2009), DOI(<https://doi.org/10.1016/j.jallcom.2008.12.081>)
- [17] R. A. Rodríguez, N. D. S. Mohallem, M. A. Santos, D. A. S. Costa, L. A. Montoro, Y. M. Laffita, E. L. Perez-Cappe, Unveiling the role of Mn-interstitial defect and particle size on the Jahn-Teller distortion of the LiMn_2O_4 cathode material, Journal of Power Sources, 490, 229519(2021), DOI(<https://doi.org/10.1016/j.jpowsour.2021.229519>)



- [18] W. Xu, Y. Zheng, Y. Cheng, R. Qi, H. Peng, H. Lin, R. Huang, Understanding the effect of Al doping on the electrochemical performance improvement of the LiMn_2O_4 cathode material, *ACS Applied Materials & Interfaces*, 13(38), 45446-45454(2021), DOI(<https://doi.org/10.1021/acsami.1c11315>)
- [19] R. Chen, B. Wen, H. Li, M. Xiang, C. Su, J. Guo, Z. Sa, Facile preparation of high-performance spinel $\text{LiMn}_{2-x}\text{Cu}_x\text{O}_4$ cathodes by microwave-induced solution flameless combustion, *Vacuum*, 187, 110077(2021), DOI(<https://doi.org/10.1016/j.vacuum.2021.110077>)
- [20] D. Arumugam, G. P. Kalaignan, K. Vediappan, C. W. Lee, Synthesis and electrochemical characterizations of nano-scaled Zn doped LiMn_2O_4 cathode materials for rechargeable lithium batteries, *Electrochimica Acta*, 55(28), 8439-8444(2010), DOI(<https://doi.org/10.1016/j.electacta.2010.07.033>)
- [21] Q. Yu, P. Li, Q. Guo, Synthesis and Properties of the LiMn_2O_4 Cathode Material for Lithium-ion Batteries, *International Research Journal of Pure and Applied Chemistry*, 25(3), 14-21(2024), DOI([10.1088/2752-5724/ad9e08](https://doi.org/10.1088/2752-5724/ad9e08))
- [22] H. J. Guo, X. Q. Li, F. Y. He, X. H. Li, Z. X. Wang, W. J. Peng, Effects of sodium substitution on properties of LiMn_2O_4 cathode for lithium ion batteries, *Transactions of Nonferrous Metals Society of China*, 20(6), 1043-1048(2010), DOI([https://doi.org/10.1016/S1003-6326\(09\)60255-7](https://doi.org/10.1016/S1003-6326(09)60255-7))
- [23] Y. C. Chen, K. Xie, Y. Pan, C. M. Zheng, H. L. Wang, High power nano- LiMn_2O_4 cathode materials with high-rate pulse discharge capability for lithium-ion batteries, *Chinese Physics B*, 20(2), 028201(2011), DOI([10.1088/1674-1056/20/2/028201](https://doi.org/10.1088/1674-1056/20/2/028201))
- [24] C. Zhu, A. Nobuta, G. Saito, I. Nakatsugawa, T. Akiyama, Solution combustion synthesis of LiMn_2O_4 fine powders for lithium ion batteries, *Advanced Powder Technology*, 25(1), 342-347(2014), DOI(<https://doi.org/10.1016/j.apt.2013.05.015>)
- [25] O. A. Hussein, Synthesis and Characterization of (Polypyrrole-Ferrites) Nanocomposites for Multi-Applications, Ph.D. Thesis, University of Diyala, Diyala, Iraq, (2022)



- [26] C. Peng, J. Huang, Y. Guo, Q. Li, H. Bai, Y. He, J. Guo, Electrochemical performance of spinel $\text{LiAl}_x\text{Mn}_{2-x}\text{O}_4$ prepared rapidly by glucose-assisted solid-state combustion synthesis, *Vacuum*, 120, 121-126(2015),
DOI(<https://doi.org/10.1016/j.vacuum.2015.07.001>)
- [27] L. Mao, S. Du, S. Li, Z. Ren, Excellent stability of Al-doped LiMn_2O_4 prepared by a sol-gel method, In 2016 5th International Conference on Environment, Materials, Chemistry and Power Electronics, Atlantis Press, (2016),
DOI(<https://doi.org/10.2991/emcpe-16.2016.72>)
- [28] M. Ahmad, M. Shahid, Y. M. Alanazi, A. ur Rehman, M. Asif, C. W. Dunnill, Lithium ferrite ($\text{Li}_{0.5}\text{Fe}_{2.5}\text{O}_4$): synthesis, structural, morphological and magnetic evaluation for storage devices, *Journal of materials research and technology*, 18, 3386-3395(2022),
DOI(<https://doi.org/10.1016/j.jmrt.2022.03.113>)
- [29] J. I. Goldstein, D. E. Newbury, J. R. Michael, N. W. Ritchie, J. H. J. Scott, D. C. Joy, *Scanning electron microscopy and X-ray microanalysis*, Springer, (2017)
- [30] H. T. Homada, N. M. Alia, O. A. Al-Jubourib, M. H. Al-Timimia, Synthesis and characterization of $\text{LiCo}_{1-x}\text{Ni}_x\text{O}_2$ nanoparticles by urea route as cathode for lithium-ion battery, *Journal of Ovonic Research*, 19(6), 783-791(2023),
DOI(<https://doi.org/10.15251/JOR.2023.196.783>)
- [31] N. Elgrishi, K. J. Rountree, B. D. McCarthy, E. S. Rountree, T. T. Eisenhart, J. L. Dempsey, A practical beginner's guide to cyclic voltammetry, *Journal of chemical education*, 95(2), 197-206(2018), DOI(<https://doi.org/10.1021/acs.jchemed.7b00361>)
- [32] J. Abou-Rjeily, I. Bezza, N. A. Laziz, C. Autret-Lambert, M. T. Sougrati, F. Ghamouss, High-rate cyclability and stability of LiMn_2O_4 cathode materials for lithium-ion batteries from low-cost natural $\beta\text{-MnO}_2$, *Energy Storage Materials*, 26, 423-432(2020)
- [33] H. Song, Y. Liu, C. Zhang, C. Liu, G. Cao, Mo-doped LiV_3O_8 nanorod-assembled nanosheets as a high performance cathode material for lithium ion batteries, *Journal of Materials Chemistry A*, 3(7), 3547-3558(2015),
DOI(<https://doi.org/10.1039/C4TA05616G>)



- [34] J. L. Wang, Z. H. Li, J. Yang, J. J. Tang, J. J. Yu, W. B. Nie, Q. Z. Xiao, Effect of Al-doping on the electrochemical properties of a three-dimensionally porous lithium manganese oxide for lithium-ion batteries, *Electrochimica acta*, 75, 115-122(2012), DOI(<https://doi.org/10.1016/j.electacta.2012.04.136>)
- [35] M. Madhu, A. Venkateswara Rao, S. Mutyala, La and Ni Co-doping effect in LiMn_2O_4 on structural and electrochemical properties for lithium-ion batteries, *Journal of Electronic Materials*, 50(9), 5141-5149(2021), DOI(<https://doi.org/10.1007/s11664-021-09037-w>)
- [36] J. Zhang, J. Shen, Shen, C. Wei, H. Tao, Y. Yue, Synthesis and enhanced electrochemical performance of the honeycomb $\text{TiO}_2/\text{LiMn}_2\text{O}_4$ cathode materials, *Journal of Solid State Electrochemistry*, 20, 2063-2069(2016), DO(<https://doi.org/10.1007/s10008-016-3197-4>)
- [37] A. C. Lazanas, M. I. Prodromidis, Electrochemical Impedance Spectroscopy, A tutorial, *ACS Measurement Science Au*, (2023), DOI(<https://doi.org/10.1021/acsmeasuresciau.2c00070>)
- [38] H. Sharifi, B. Mosallanejad, M. Mohammadzad, S. M. Hosseini-Hosseinabad, S. Ramakrishna, Cycling performance of $\text{LiFePO}_4/\text{graphite}$ batteries and their degradation mechanism analysis via electrochemical and microscopic techniques, *Ionics*, 1-16(2022), DOI(<https://doi.org/10.1007/s11581-021-04258-9>)
- [39] S. Priyono, S. Hardiyani, Hardiyani, N. Syarif, A. Subhan, A. Suhandi, Electrochemical performance of LiMn_2O_4 with varying thickness of cathode sheet, In *Journal of Physics: Conference Series* 1191(1), 012022 (2019), DOI([10.1088/1742-6596/1191/1/012022](https://doi.org/10.1088/1742-6596/1191/1/012022))
- [40] J. Zeng, M. Li, X. Li, C. Chen, D. Xiong, L. Dong, X. Sun, A novel coating onto LiMn_2O_4 cathode with increased lithium ion battery performance, *Applied surface science*, 317, 884-891(2014), DOI(<https://doi.org/10.1016/j.apsusc.2014.08.034>)
- [41] K. F. Qasim, W. A. Bayoumy, and M. A. Mousa, Electrical and electrochemical studies of core-shell structured nanorods of $\text{LiMn}_2\text{O}_4@\text{PANI}$ composite, *Journal of Materials Science: Materials in Electronics*, 31(22), 19526-19540(2020), DOI(<https://doi.org/10.1007/s10854-020-04482-5>)



- [42] Y. G. Guo, J. S. Hu, and L. J. Wan, Nanostructured materials for electrochemical energy conversion and storage devices, *Advanced Materials*, 20(15), 2878-2887(2008), DOI(<https://doi.org/10.1002/adma.200800627>)
- [43] X. Xiao, L. Wang, D. Wang, X. He, Q. Peng, and Y. Li, Hydrothermal synthesis of orthorhombic LiMnO_2 nano-particles and LiMnO_2 nanorods and comparison of their electrochemical performances, *Nano Research*, 2, 923-930(2009), DOI(<https://doi.org/10.1007/s12274-009-9094-8>)